Journal of Power Technologies 104 (2) (2024) 99 -- 115

Analysis and Comparison of SVPWM and SPWM Methods Used for Indirect Rotor Flux-Oriented Control of EV Applications

Amir Arsalan Astereki [1], Pouria Changalvaie nia [1], Mehdi Monadi[1,] ✉

[1] Shahid Chamran University of Ahvaz, Faculty of Engineering, Ahvaz, Iran

✉Corresponding author. Email: m.monadi@scu.ac.ir

Abstract

Nowadays, electric vehicles (EVs) are considered one of the best solutions to reduce fossil-fuel usage in the transportation industry. In EV applications, due to the cost and maintenance problems, induction motors (IMs) are exciting option over DC motors. Therefore, IM power-electronic-based drives are the EVs most essential components which need more consideration and investigation. One of the effective and well-known control methods in AC electric motor drives is the indirect rotor flux-oriented control (IRFOC) method. The IRFOC method controls the electromagnetic torque and rotor flux independently. The IRFOC method should be equipped with a proper switching technique to reduce power losses, disturbances, voltage/current distortions, etc. The Sinusoidal Pulse Width Modulation (SPWM), and Space Vector Pulse Width Modulation (SVPWM) methods are of the available switching methods for electric motor drives. Few studies have been conducted to compare these two switching methods, but less focus has been on their effects on EV performance when a vehicle's parameters, such as load torque, are changed. In this paper, the mentioned switching strategies are simulated to control a 50 hp, 460V three-phase induction motor. The required simulations were done in the MATLAB/ Simulink software, and several scenarios were considered to compare the performance of SPWM and SVPWM methods in terms of speed tracking, disturbances created by the drive converter, efficiency, input and output power, required DC battery, and the EV motor stability under load change. The merits and drawbacks of these two switching methods are also described in detail.

Keywords: Electric drive, sinusoidal PWM, space vector PWM, indirect rotor flux-oriented control, electric vehicles.

1. Introduction

Nowadays, EVs have attracted more interest than conventional gasoline cars because of their effects on greenhouse gas reductions [1-3]. Although depending on the vehicle applications, various types of electric motors have been used for EVs, the usage of induction motors (IM) is more frequent in EV industries [4]. Indeed, IMs are used in EVs due to their simple structure, strength, low-cost production, ease of manufacture, and fault-tolerant properties [5]. Researchers around the world are working on proposing and using more precise control methods for EV's drives [6]. Of course, it should be noted that using simple methods, that are presented for DC motors precise torque control cannot be easily achieved in IM [7]. Many control strategies are presented for IM drives based on methods such as conventional proportional integral derivative (PID) [8], Fuzzy Logic Controller (FLC), as well as scalar control methods, e.g., the voltage to frequency (V/F) [9]. The V/F method was widely used due to its simplicity; however, the method provides a slow response, and cannot be used when precise speed control is needed [10]. To enhance the dynamic response of the IMs, decoupled flux control methods like vector control and direct torque (DTC), are also suggested [11]. However, conventional DTC may

drop the IM airgap flux, typically at low speeds [12]. The field orientation control (FOC) method was also presented for IM drives. The FOC method is separated into two methods called direct field orientation control (DFOC), and indirect field orientation control (IFOC). The implementation of DFOC requires special sensors such as hall-effect sensors. Using these sensors, not only increases the controller cost and reduces the reliability but also may cause some extra control issues [13]. However, the IFOC does not need the flux observer/estimator or the flux linkage sensor [14, 15]. Noted that, from the above-mentioned control methods, the IFOC and the DTC are the most commonly used methods to control the IMs [16]. In the IFOC method, the torque-generating current decouples from the flux-generating current [17]; therefore, by using this method, the motor torque is controlled independently. In this method, the desired torque is produced by comparing the desired motor speed, determined by the vehicle driver, with the actual EV speed. Then, the proper control signals are sent to the PWM generators to generate the related switching signals of the EV inverter.

On the other hand, the torque ripple and disturbed motor voltage/current, caused due to the switching behavior of the EV inverters, may apply mechanical stresses to the vehicle. [18]. Furthermore, the converter's fast switching can cause electromagnetic interference issues which in turn affect the operation of the EV's electrical systems, including IM and controlling circuits [19]. Accordingly, from this point of view, it is necessary to select a proper PWM-based switching technique for the vehicle's IM drive to guarantee the stable operation of the EVs.

The PWM technique generally works based on comparing a sinusoidal reference and a triangular carrier waveforms [8]. In this method, the frequencies and the magnitudes of the inverter output voltage can be controlled by changing the modulation coefficients [20]. The two well-known methods of PWM techniques in the literature are the SPWM and the SVPWM. The SPWM provides several advantages, such as lower harmonic distortion and power losses, as well as simple implementation. Moreover, by using this method, the EV's inverter can operate in the fixed switching frequency mode [21]. On the other hand, SVPWM may provide smaller current distortion, and reduction of torque and flux linkage pulsation. The SVPWM also can be implemented easily in the controllers of the IM's inverters [22, 23]. To select a proper witching method for the EV's motor drive, it is essential to compare and analyze these two methods, comprehensively.

Some comparisons between SPWM and SVPWM can be found in the literature; however, most were only focused on a limited number of these technique's aspects. For instance, in [24], only the current THD of these methods is compared; while in [25], the performance of SPWM, and SVPWM were compared in terms of the load torque and the motor speed. In [26-28] the output THD, rising time, speed tracking, and stator currents, were compared; however, the other operational aspects of the SVPWM and SPWM were not considered. Also, the comparison reported in [29] has considered the efficiency of two different drives that work based on SPWM and SPVWM. But, this comparison was not done according to the specifications of EV's IM. Indeed, the above-mentioned works cannot provide a comprehensive comparison between SVPWM and SPWM when they are used to drive the IMs of the EVs.

Accordingly, this paper presents a comprehensive comparison between SPWM and SVPWM techniques that are used for IRFOC-based drives of EVs. This comparison can be useful for academic and industrial researchers who work on the EV's power electronic drives. The comparison investigates a wide range of operational aspects of EV's drives such as inverter output THD, motor efficiency, motor power factor, speed tracking,

overshoots, rising time, and the required battery under various load and torque/speed reference changes.

The rest of the paper is organized as follows. Section II represents the basics of the vehicle dynamics. The IRFOC concept is introduced, and the overall scheme of the IM drives used in EVs is explained in Section III. Sections IV and V introduce the SPWM and the SVPWM switching methods, respectively. In Section VI, the required battery pack voltage for the mentioned switching methods is discussed. In Section VII a 50 hp three-phase induction motor, whose power is enough for EV application, is simulated in MATLAB/ Simulink. Matlab/ Simulink was already used in many related works, such as the work presented in [30], due to its capability in simulating power converters and their controllers. During the simulation-based study, the effects of changing various system parameters are compared when SPWM or SVPWM is employed as a switching technique.

2. VEHICLE DYNAMICS

The propelling force between the wheels and the line surface controls the vehicle acceleration [31]. This propelling force should be provided by the EV's IM and be controlled by the related drive. Therefore, the EV drives should be designed properly to be able to generate the forces needed for EV movement in the various operational conditions. In this regard, to calculate the total tractive force needed for the vehicle's movement, it is necessary to know the EV dynamics. Indeed, to evaluate the EV performance, to improve the size of the IM, and to enhance the energy efficiency, the EV dynamics must be modeled, first. The equations (1-8) describe the EV dynamics [31-34].

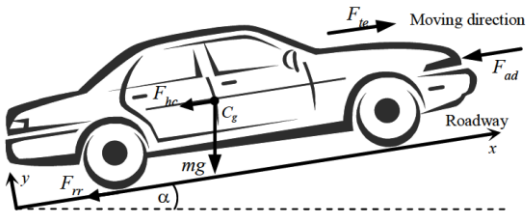

Figure1: The total forces acting on the electric vehicle [32].

By considering an EV as a mass, m, that moves with speed v upward on a road that its slope angle is α, the total forces acting on the EV are depicted in Figure 1. The motor acceleration can be calculated as:

$$\frac{dv}{dt} = \frac{\sum f_e - \sum f_r}{\mu m} \quad (1)$$

where $\sum f_e$ is the sum of tractive efforts, $\sum f_r$ is the sum of resistive forces (including aerodynamic drag, rolling friction, and EV weight), and μ is the mass factor.

To accelerate the EV, the tractive force from the front and rear wheels, labeled as f_{tf} and f_{tr} should overcome the net resistive force. The rolling resistance, F_{rr}, is caused by the flattening of the tire at the contact surface of the road [33].

$$F_{rr} = \mu_1 mgcos(\propto) + \mu_2 N_r v \quad (2)$$

Note that, μ_1 depends on tire pressure and tire type, while the μ_2 is an almost constant coefficient for EVs. The aerodynamic drag force, f_{ad}, is another resistive force that is related to the air viscous resistance on the EV surface.

$$F_{ad} = \frac{1}{2}\rho CA(v + v_0)^2 \quad (3)$$

Where ρ is the air density, C is an aerodynamic coefficient, A is the EV frontal area, and v_0 is the headwind velocity. Moreover, the EV weight causes a resistive force, f_{hc}, to align with the road slope, which is calculated as:

$$F_{hc} = \pm mg\sin(\alpha) \quad (4)$$

If the EV speed changes, the additional linear force appears, which is called inertia force, and is calculated as:

$$F_{inr} = \mathrm{m}\frac{dv}{dt} \quad (5)$$

accordingly, equation (1) can be rewritten as follows.

$$m\mu\frac{dv}{dt} = (f_{tf} + f_{tr}) - (f_{rr} + f_{inr} + f_{ad} + f_{hc}) \quad (6)$$

Moreover, the rotor speed reference and the applied load torque to the motor shaft, from the gearbox, can be achieved by the following equations.

$$T_l = \frac{r_d}{k_g k_o \eta_d}(f_{rr} + f_{ad} + f_{hc}) \quad (7)$$

$$\omega_r{}^* = \frac{30 k_g k_o v_r}{\pi r_d} \quad (8)$$

where $\boldsymbol{r_d}$ is the effective radius of the tire, and $\boldsymbol{k_g}$ and $\boldsymbol{k_o}$ are the transmission and the final drive gear ratios, respectively. In addition, $\boldsymbol{\eta_d}$ is the efficiency of the drive, $\boldsymbol{T_l}$ is the load torque, $\boldsymbol{\omega_r}^*$ is the rotor angular speed reference, and $\boldsymbol{v_r}$ is the driver speed reference.

3. INDIRECT ROTOR FLUX-ORIENTED CONTROL

As mentioned above, to control the Evs electric motors, several control methods like IRFOC, switching table-based direct torque control (ST-DTC), and predictive torque control (PTC) are already presented. The IRFOC is selected in many applications because of its fast dynamics response. Moreover, using this method the torque and the flux can be controlled, independently [35]. The concepts of the vector control method, also known as field-orientated control (FOC), have been proposed in many articles. The logic of the vector control is controlling an IM similar to the control principle of a separately excited DC motor that torque and magnetic flux are controlled independently [36]. In this method, the stator current is decupled into two components called the direct axis component (***ids***) and quadrature axis component (***iqs***); these components of the inverter current are controlled separately. The ***ids*** is in the direction of flux linkage, and the ***iqs*** is orthogonal. To properly understand the method, it is essential to outline the dynamics of the induction machine.

A. Dynamic model of Three-phase IM

The dynamic model of an IM in the synchronously rotating reference frame is shown in Figure 2.

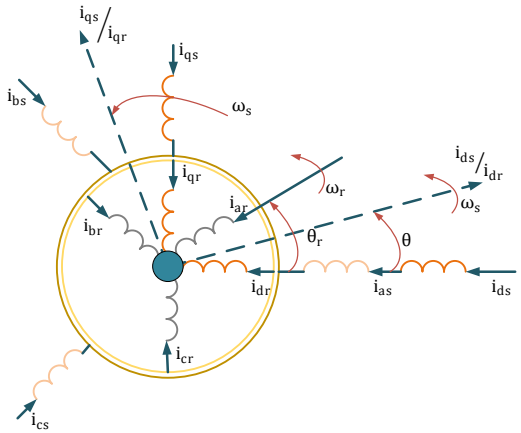

Figure2: The dynamic model of an IM [26].

According to Figure 2, the flux linkages and the voltages of a three-phase induction motor, in ***dq*** frame, are given by the following equations [37, 38].

$$\lambda_{ds} = L_S i_{ds} + L_m i_{dr} \quad (9)$$

$$\lambda_{qs} = L_S i_{qs} + L_m i_{qr} \quad (10)$$

$$\lambda_s = \sqrt{{\lambda_{ds}}^2 + {\lambda_{qs}}^2} \quad (11)$$

$$\lambda_{dr} = L_r i_{dr} + L_m i_{ds} \quad (12)$$

$$\lambda_{qs} = L_r i_{qr} + L_m i_{qs} \quad (13)$$

$$\lambda_r = \sqrt{{\lambda_{dr}}^2 + {\lambda_{qr}}^2} \quad (14)$$

Where, the $\boldsymbol{\lambda_{dqr}}$ and $\boldsymbol{\lambda_{dqs}}$ are the flux linkages of the rotor, and the stator; $\boldsymbol{L_m}$, $\boldsymbol{L_r}$ and $\boldsymbol{L_S}$ are the mutual, the rotor and the stator inductances. Moreover, the voltages of a three-phase induction motor can be expressed as follows [37, 38].

$$v_{ds} = R_s i_{ds} + \frac{d}{dt}(\lambda_{ds}) - \omega_e \lambda_{qs} \quad (15)$$

$$v_{qs} = R_s i_{qs} + \frac{d}{dt}(\lambda_{qs}) + \omega_e \lambda_{ds} \quad (16)$$

$$v_{dr} = R_r i_{dr} + \frac{d}{dt}(\lambda_{dr}) - (\omega_e - \omega_r)\lambda_{qr} \quad (17)$$

$$v_{qr} = R_r i_{qr} + \frac{d}{dt}(\lambda_{qr}) + (\omega_e - \omega_r)\lambda_{dr} \quad (18)$$

Where, $\boldsymbol{v_{dr}}$, $\boldsymbol{v_{qr}}$, $\boldsymbol{v_{ds}}$ and $\boldsymbol{v_{qs}}$ are the rotor and stator voltages in the $\boldsymbol{dq}$ frame, $\boldsymbol{\omega_e}$ is the synchronous speed, $\boldsymbol{R_r}$ and $\boldsymbol{R_s}$ are the winding resistances of the rotor and stator, and $\boldsymbol{\omega_r}$ is the rotor speed.

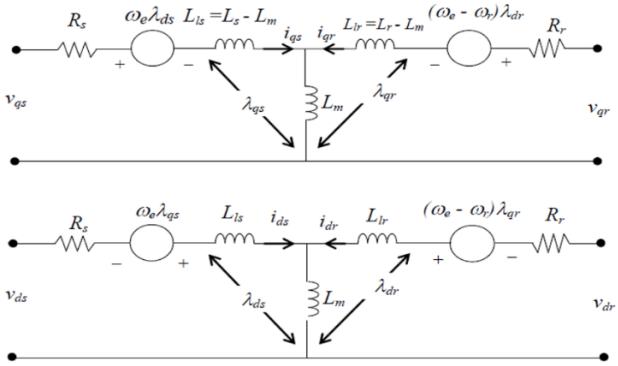

Figure 3: The dynamic equivalent circuits of an IM in the dq frames [37].

Accordingly, the dynamic equivalent circuits of a three-phase IM in the $\boldsymbol{dq}$ frames are shown in Figure 3. Moreover, the mechanical output power and the developed electromagnetic torque are given by equation 19 and equation 20, respectively [38].

$$P_m = \frac{3}{2}[\omega_r \lambda_{ds} i_{qs} - \omega_r \lambda_{qs} i_{ds}] \quad (19)$$

$$T_{dev} = \frac{P_m}{\omega_r / P} = \frac{3}{2} P L_m (i_{dr} i_{qs} - i_{qr} i_{ds}) \quad (20)$$

Where $\boldsymbol{P}$ is the number of pole pairs. According to [38], the torque of the motor in the $\boldsymbol{dq}$ frame is given by:

$$\mathcal{T}_e = \frac{3}{2} P \frac{L_m}{L_r} (\lambda_{dr} i_{qs} - \lambda_{qr} i_{ds}) \quad (21)$$

B. Rotor-Flux Orientation Control

The use of the rotor-flux orientation method is more usual because of its simple design [38]. In this method, the flux position is determined from the motor equivalent model, and the rotor flux is oriented to the d-axis [39]. Indeed, the q-axis component of the flux is always zero.

It is noted that if the angle between $\bar{\boldsymbol{\lambda}}_{\boldsymbol{s}}$ or $\bar{\boldsymbol{\lambda}}_{\boldsymbol{r}}$ and $\bar{\boldsymbol{is}}$ is made to be 90°, then the IM behaves similarly to a DC motor. This angle difference is achieved by selecting the orientation

(alignment) of the rotating **dq** frame on $\boldsymbol{\lambda_s}$ or $\boldsymbol{\lambda_r}$. In this case, the direct axis component of $\boldsymbol{i_s}$ is align with the rotor flux linkage. Figure 4 demonstrates the orientations of the IRFOC method in which the **dq** frame rotates at $\boldsymbol{\omega_s}$ speed.

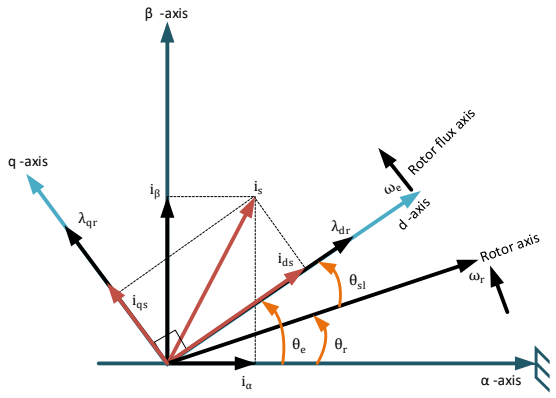

Figure 4: The rotor flux vector diagram [23].

By assuming the rotor flux direction along $\boldsymbol{i_s}$, it could be shown that $\lambda_{qr} = 0, and\ \lambda_{dr} = |\lambda_r|$. Also, the electromagnetic torque is [38]:

$$\mathcal{T}_e = \frac{3}{2} P \frac{L_m}{L_r} (\lambda_{dr} i_{qs}) \tag{22}$$

According to equation 22, the electromagnetic torque is proportional to the rotor flux linkage and the stator q-axis current. If the rotor flux linkage has remained constant, the torque is proportional to the torque-producing component of the stator current ($\boldsymbol{i_{qs}}$). Assuming $\lambda_{qr} = 0$, the equations of the dynamic model of three-phase IM in the rotor flux orientation are as follows [38].

$$v_{ds} = R_s i_{ds} + \sigma L_s \frac{d}{dt} i_{ds} - \omega_s \sigma L_s i_{qs} + \omega_s \frac{L_m}{L_r} \frac{d}{dt} \lambda_{dr} \tag{23}$$

$$v_{qs} = R_s i_{qs} + \sigma L_s \frac{d}{dt} i_{qs} + \omega_s \sigma L_s i_{ds} + \omega_s \frac{L_m}{L_r} \lambda_{dr} \tag{24}$$

$$v_{dr} = 0 = \frac{R_r}{L_r} \lambda_{dr} + \frac{d}{dt} \lambda_{dr} - \frac{L_m}{L_r} R_r i_{ds} \tag{25}$$

$$v_{qr} = 0 = \omega_{sl} \lambda_{dr} - \frac{L_m}{L_r} R_r i_{qs} \tag{26}$$

$$\sigma = 1 - \frac{L_m{}^2}{L_S L_r} \tag{27}$$

Where the $\boldsymbol{L_r}$ is the rotor inductance referred to the stator side, and $\boldsymbol{\omega_{sl}}$ is the slip angular frequency. Thus, by defining $\boldsymbol{\lambda_{dr}}$ in equation 28, the following equations can be achieved:

$$\lambda_{dr} = L_m i_{mrd} \tag{28}$$

$$i_{ds} = i_{mrd} + \frac{L_r}{R_r} \frac{d}{dt} i_{mrd} \tag{29}$$

$$i_{ds} = i_{mrd}(1 + S\tau) \tag{30}$$

$$\tau = \frac{L_r}{R_r} \tag{31}$$

Where $\boldsymbol{i_{mrd}}$ is called the "equivalent magnetizing current" or "field current".

According to equations 28 and 30, it can be said that the flux and the magnetism production can be controlled by $\boldsymbol{i_{ds}}$. This concept confirms the previous vector diagram.

As mentioned before, the ***dq*** frame rotates at $\boldsymbol{\omega_s}$, hence:

$$\theta^{\lambda_r} = \int \omega_s \, dt \tag{32}$$

In the indirect method, the flux angle is estimated from the measured speed, without

the requirements of measuring the electrical quantities. Accordingly:

$$\theta^{\lambda_r} = \int (\omega_{sl} + \omega_r)\, dt \tag{33}$$

$$\omega_{sl} = \frac{L_m}{L_r}\frac{R_r}{\lambda_{dr}} i_{qs} = \frac{i_{qs}}{\tau \times i_{mrd}} \tag{34}$$

Hence, by choosing desire $\boldsymbol{\lambda_{dr}}^*$ and $\boldsymbol{T_e}^*$, as the references, the $\boldsymbol{i_{ds}}^*$, $\boldsymbol{i_{qs}}^*$ and $\boldsymbol{\theta_e}$ can be obtained from equation 35 to equation 40; these parameters are then used as the reference values of the IRFOC method.

$$i_{mrd}{}^* = \frac{\lambda_{dr}{}^*}{L_m} \tag{35}$$

$$i_{sd}{}^* = (1 + \tau s) i_{mrd}{}^* \tag{36}$$

$$\theta^{\lambda_r} = \int (\omega_{sl} + \omega_r)\, dt \tag{37}$$

$$i_{qs}{}^* = \frac{T_e{}^*}{k_t \times i_{sd}{}^*} \tag{38}$$

$$k_t = \frac{3}{2}\frac{p}{2}\frac{{L_m}^2}{L_r} \tag{39}$$

$$\omega_{sl} = \frac{i_{qs}}{\tau \times i_{mrd}} \tag{40}$$

Where $\boldsymbol{k_t}$ is a constant coefficient. As it is shown in Figure 5, the stator currents reference (i.e., $\boldsymbol{i_{ds}}^*$, $\boldsymbol{i_{qs}}^*$) are compared with the actual stator currents, and then the related error is fed to a PI controller to make the proper signals for the SVPWM or SPWM generator. Then, the proper signals are sent to IM drive converter switches to control the torque or rotor flux. Moreover, to generate the electromagnetic torque reference, another PI controller can be added. This PI controller works on the difference values of the reference speed and the actual speed to generate a proper reference signal for the electromagnetic torque [40]. The overall scheme of the IRFOC control scheme with both switching methods is presented in Figure 5.

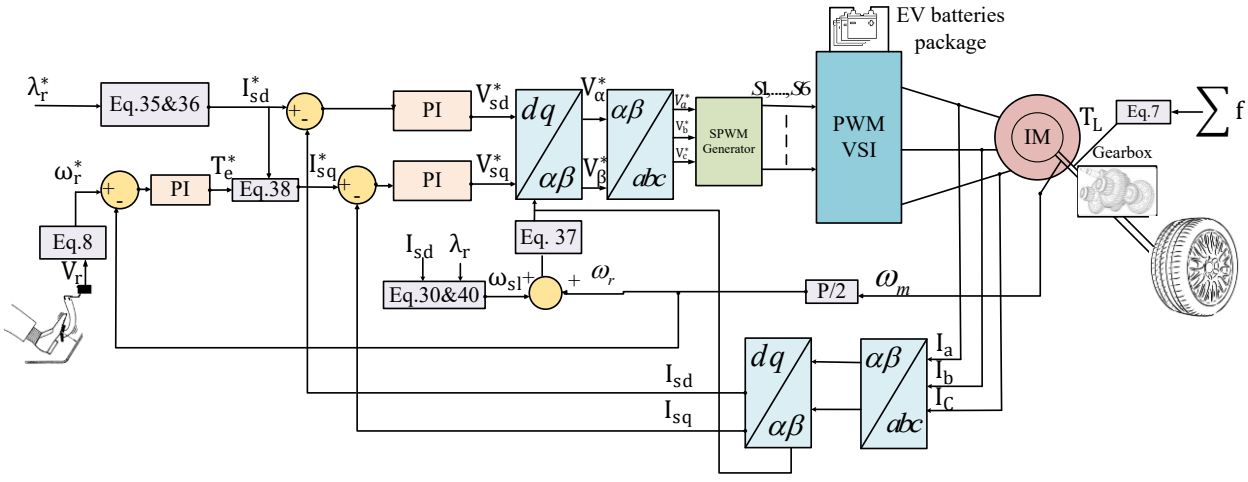

(a)

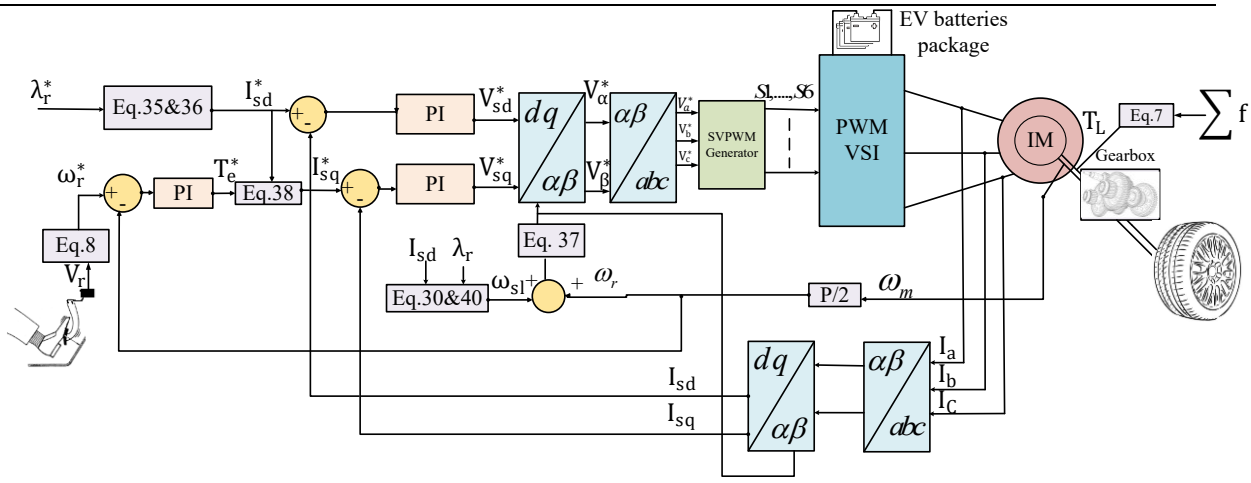

Figure 5: The overall scheme of the proposed EV control system with both switching methods. a) SPWM method, b) SVPWM method.

4. SINUSOIDAL PULSE WIDTH MODULATION

As shown in Figure 6, in the SPWM method, the switching signals are generated based on comparing a sinusoidal reference signal with a triangular carrier waveform [41]. The frequency of the sinusoidal modulating signal is set at the fundamental frequency (e.g., 60Hz) of the desired output voltage.

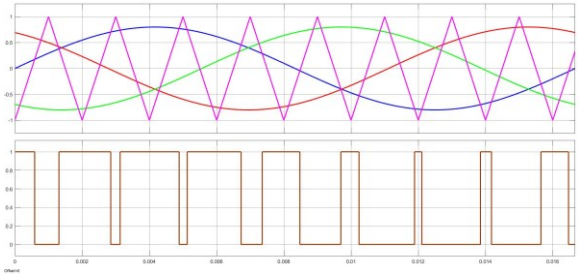

Figure 6: Principle of sinusoidal PWM of three-phase bridge inverter [37].

5. SPACE VECTOR PULSE WIDTH MODULATION

The SVPWM is another modulation technique in which the inverter switching states are determined in a space vector. Indeed, in the SVPWM method, a space vector, in the Clarke reference domain, is assigned for each converter switching state. There are eight voltage vectors, including two zero voltage vectors called ***V0*** and ***V7***, and six other vectors called ***V1***, ***V2***, ***V3***, ***V4***, ***V5***, and ***V6***, which are named active voltage vectors. Each of these vectors has a fixed magnitude and is 60˚ apart from other adjacent vectors. The reference voltage vector is resolved into a combination of these eight voltage vectors. This means that the required output voltage is produced by switching between the two nearest vectors and a zero vector [42, 43].

According to [44], space vector representation of three-phase quantities $\boldsymbol{V_a(t)}, \boldsymbol{V_b(t)}$ and $\boldsymbol{V_c(t)}$ with space distribution of 120^o is given by:

$$\bar{V}_s = \frac{2}{3}[V_a(t) + \alpha V_b(t) + \alpha^2 V_c(t)] \qquad (42)$$

where

$$\alpha = e^{j2\pi/3} = \cos\left(\frac{2\pi}{3}\right) + j\sin\left(\frac{2\pi}{3}\right) \quad \text{and} \quad \alpha^2 = e^{j4\pi/3} = \cos\left(\frac{4\pi}{3}\right) + j\sin\left(\frac{4\pi}{3}\right).$$

If $\boldsymbol{V_a}$, $\boldsymbol{V_b}$, and $\boldsymbol{V_c}$ are 3-phase balanced sinusoidal voltage, with the frequency of $\boldsymbol{f}$, the locus of $\bar{\mathbf{v}}_s$

is circular that its radius is equal to the peak value of the phase voltage. Moreover, $\mathbf{v_s}$ rotates with an angular speed of $2\pi f$. Accordingly, the $\bar{V}_s$ can be rewritten as follow:

$$\bar{V}_s = \frac{2}{3} V_{dc}[S_a + \alpha S_b + \alpha^2 S_c] \qquad (43)$$

where $\boldsymbol{S_a}$ is the switching condition of the first leg of the inverter, and $\boldsymbol{S_b}$ and $\boldsymbol{S_c}$ are the switching conditions of the second and third inverter legs. The value of each $\boldsymbol{S}$ can be 1 or 0, and $\boldsymbol{V_{dc}}$ is the DC link source voltage. Therefore, eight inverter states can be obtained. The operating states and corresponding vectors are listed in Table 1 and shown in Figure 7.

Table 1: Switching states of the two-level three-phase inverter [45].

Space vector	Switching state	'On' switches S*i*
V7	[111]	1,3,5
V0	[000]	4, 6, 2
V1	[001]	4, 6, 5
V2	[010]	4,3,2
V3	[011]	4,3,5
V4	[100]	1,6,2
V5	[101]	1,6,5
V6	[111]	1,3,2

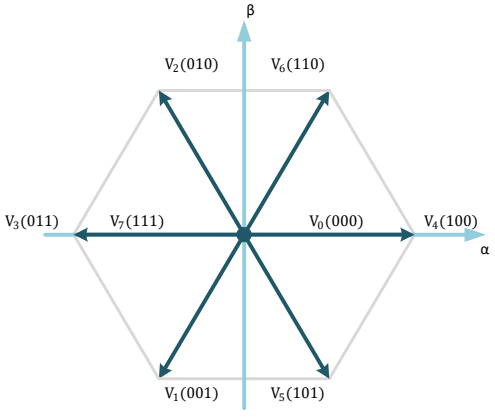

Figure 7: Vectors in the SVPWM method [45].

6. REQUIRED EV BATTERY VOLTAGE

As mentioned, the DC link voltage is needed to supply the inverter through a battery pack. The battery pack of EVs consists of several parallel and series cells. By putting the battery cells in series, the high desired DC link voltage will be gained [46]. Another way to increase the DC link voltage is to employ a DC/DC converter with bidirectional power flow capability [47]. It is clear that a lower required DC link voltage needs fewer battery cells in series and therefore reduces the battery pack size and price. The SVPWM and SPWM methods are compared here in terms of the required DC voltage, and the required battery cell when they are feeding the same IM.

In [48], for a 2-level inverter, the AC side line-to-line voltage is calculated as follows:

$$V_{L-L} = 0.612 \times M_i \times V_{dc} \qquad (44)$$

For modulation index ≤ 1, the battery voltage is:

$$V_{dc} \geq \frac{V_{L-L}}{0.612} \qquad (45)$$

However, a more accurate calculation for EV battery voltage is introduced in [49]. According to the method presented in [49] in the SPWM, and the SVPWM, the required DC link voltage is equal to:

$$V_{dc-spwm} = 2 \times V_{max-phase} \qquad (46)$$

$$V_{dc-svpwm} = \sqrt{3} \times V_{max-phase} \qquad (47)$$

Figure 8 shows the relation between output voltages and required DC link voltage in each switching method.

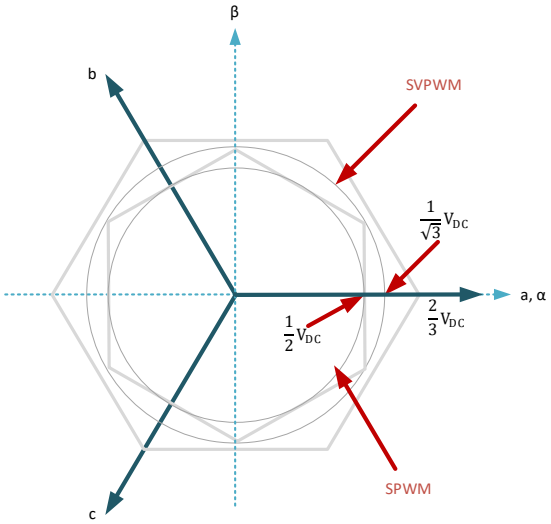

Figure 8: The DC link voltage needed for each method [49].

So, the desired EV battery voltage for the SVPWM switching method is lower than SPWM switching method. It means that by using SVPWM method less numbers of battery cells are needed to run the IM of an EV.

In the next section, an in-depth comparison between the SPWM and the SVPWM methods for the IRFOC control strategy is presented in various EV conditions.

7. SPWM AND SVPWM PERFORMANCE COMPARISON IN EV APPLICATIONS

The overall schemes of the SPWM and the SVPWM methods that are used in the IRFOC-based controller of an EV induction motor are presented in Figure 5 for a motor introduced in Table 2. To provide a comprehensive evaluation of the SPWM and the SVPWM switching methods, several case studies have been done to compare their performance in terms of speed tracking, provided electromagnetic torque, voltage and current THDs, and IM input and output powers. The required simulations have been done in MATLAB/ Simulink software. It is also noted that the PI coefficients for both cases are obtained with the frequency-response procedure presented in [50].

Table2: Motor parameters

Motor Parameters	Value
Power	50 HP
Voltage	460 V
Rated speed	1760 rpm
Frequency	60 Hz
Stator resistance Rs	0.0870 Ω
Stator Inductance Ls	0.0348 H
Moment of inertia J	0.662 kg–m2
Rated Load Torque (TL)	202 N-m
Rotor resistance Rr	0.228 Ω
Rotor Inductance Lr	0.0355 H
Mutual inductance Lm (H)	0.0347 H
Number of poles	4

7.1. Speed-tracking responses

In this case, to illustrate the speed tracking of each switching method several simulations are done. The motor start process and reaching to the nominal speed is investigated, first. In this case, assumes that a 202 N.m load is coupled to the EV motor shaft, and the EV is moving on a flat road.

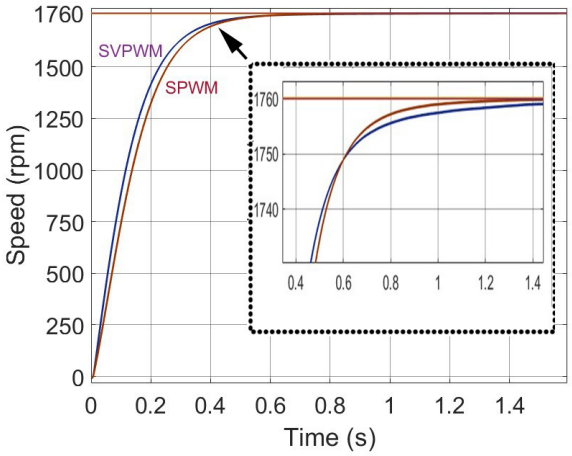

Figure 9: Comparison of speed tracking between two switching methods.

As shown in Figure 9, in this case, both switching methods show an acceptable and almost similar speed tracking behaviour. In addition, it can be seen from Figure 9 that the rising times of SVPWM and SPWM methods are around 0.23s and 0.27s, respectively. Furthermore, the settling time in the SPWM method is about 1.2s, this value is around 1.45s when SVPWM is implemented.

Moreover, to show the speed tracking performance during a step change in the speed reference, it assumed that the speed reference reduced to 1300 rpm at t=4s, then increased to 1760 rpm at t=8sec. The results of these two-step speed changes are respectively reported in Figure 11.a and 11.b. These Figures show that both switching methods control the speed, and reach 2% of error in less than two seconds.

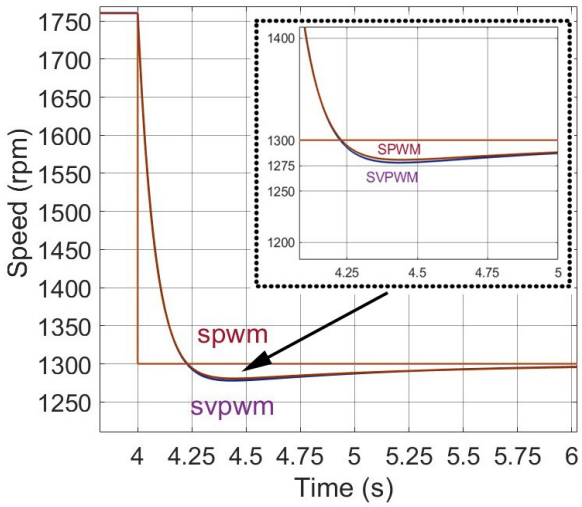

(a)

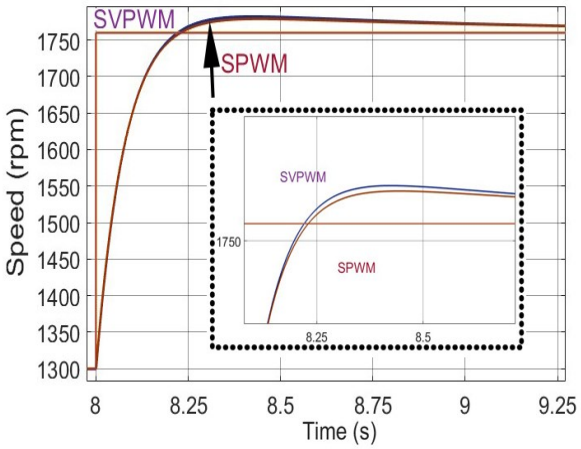

(b)

Figure 10: Speed tracking of both switching methods. a) Speed tracking during deceleration, b) Speed tracking during acceleration.

In addition, to compare the speed tracking response during the load changes, another study case was considered. In this case, it assumed that EV load changes from 202 N.m to 100 N.m at t=3s, e.g., due to the change in the road slop. Then the speed reference returns to its initial value at t=7s. During this case, the speed setpoint is set to 1500

rpm. Figure 11 shows the results of this case in which both controllers were able to stabilize the performance of the EV, and fix the motor speed after 4 seconds. However, the SVPWM provides a little bit faster damping.

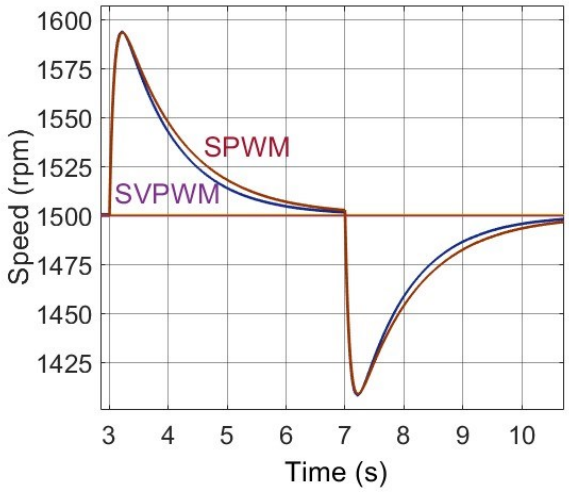

Figure 11: the speed tracking under EV load torque change.

7.2. Study the torque change under EV load changing

In this case study, the provided electromagnetic torques of both SPWM and SVPWM switching methods are compared. During this case assumed that at the rated speed, the load torque increases from 202 N.m to 100 N.m at t=3s, and then decreases from 100 N.m to 202 N.m at t=7s. Figure 12 illustrates the provided electromagnetic torque of each switching method. This figure shows that the both compared methods perform almost the same. It is also noted that, although the resistive torque is assumed to be equal to 202 N.m, the steady state value of the electromagnetic torque is about 220 N.m. The difference is due to the copper and rotational losses inside the motor.

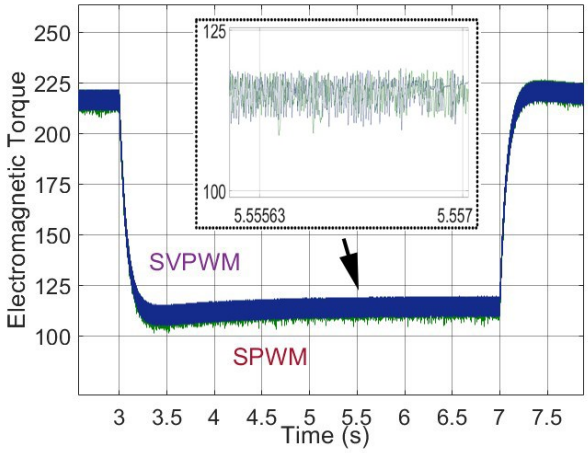

Figure 12: The electromagnetic torque changes under EV load torque change.

7.3. The motor side voltages and current harmonics

In this section, the stator currents/ voltage harmonics of the EV's IM are compared when SPWM or SVPWM methods are used in the EV controller. To present an accurate comparison, filtering components, e.g., LC harmonic filter and EMI filters, are not simulated. In addition, the switching frequency is chosen to be 5 kHz. Furthermore, the FFT analysis was used to calculate the stator voltages/ currents harmonics.

Figure 13 illustrates the calculated harmonies and the related THD values of phase ***a*** of the EV motor. It can be understood from Figure 3 that the SVPWM method causes less voltage and current harmonics. Moreover, a very high amount of THD in the voltage indicates the necessity for a harmonic filter between the inverter and the motor [20, 51].

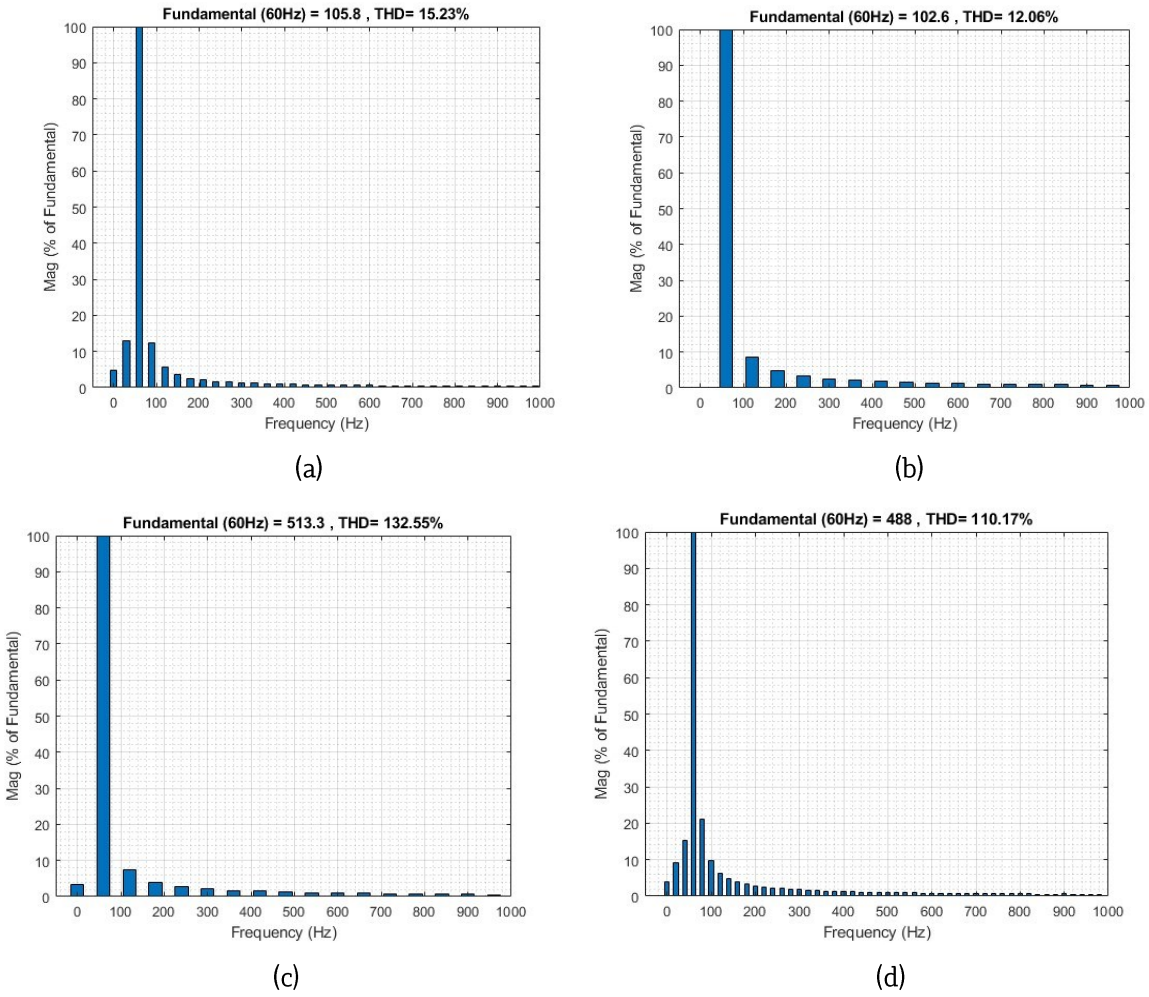

Figure 13: FFT analysis of the voltage and current of phase a for both switching methods. a) Stator current with SPWM, b) Stator current with SVPWM, c) Stator voltage with SPWM, d) Stator voltage with SVPWM

7.4. Motor Input/output power under nominal operations

Figure 14 depicts the input and output powers of the IM from the start moment to the time reaches the rated speed. In the SPWM method, the peak value of the motor power is about 120 kW, while using the SVPWM, the maximum input power reachs 150 kW. Indeed, the figure demonstrates that when the SVPWM method is used, the motor gets more power from the batteries and, consequently, produces more electromagnetic torque.

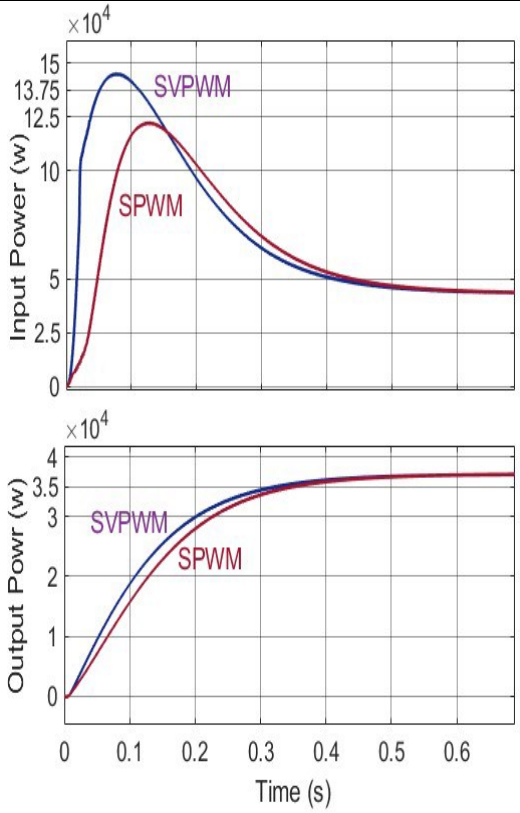

Figure 14: Input and output power of the induction motor during motor starting.

8. Comparision

Finally, to provide a more precise comparison, the overall performance of SPWM and SVPWM methods is summarized in Table 3. It can be seen from Tables 3 that, with the same motor speed and EV load torque, IM works with almost the same efficiency and power factor. However, the SVPWM method causes less voltage and current harmonics. Furthermore, to supply the IM of an EV that uses an SVPWM-based controller, a lower DC voltage is needed. This means that fewer battery cells are necessary. On the other hand, the SPWM presents a lower settling time and a lower input power peak at the starting period.

9. CONCLUSION

In this article, the performance of the EV drive controllers, which are designed based on the SPWM and the SVPWM switching techniques, were compared. These switching methods were compared in terms of speed tracking, THD, rising time, settling time, electromagnetic torque, overshoot, input and output power, efficiency, power factor, delivered torque to the motor shaft, and the required battery voltage.

The results show that although these two methods can provide almost the same characteristics in various aspects, the SVPWM method provides better performance in terms of speed response and power quality. Moreover, the implementation of this method needs a smaller battery pack which in turn reduces the weight and the size of the EV battery.

Table 3: SPWM and SPVWM Methods Comparision

parameters	SPWM	SVPWM	parameters	SPWM	SVPWM
Output Mechanical power (kW)	37.2	37.24	Load torque (N.m)	202	202
Active Input Power (kW)	43	42.98	%THD Voltage	132.55	110.17
Apparent Power(kVA)	64.38	64.23	%THD current	15.23	12.06
% Efficiency	86.5	86.64	% Overshoot	0	0

Power factor	0.667	0.669	Rise time (sec)	0.27	0.23
Required battery voltage (V)	750	650	Settling Time(sec)	1.2	1.45

REFERENCES

1. Monadi, M., et al., *Integrated control and monitoring of a smart charging station with a proposed data exchange protocol.* IET Renewable Power Generation, 2022. **16**(3): p. 532-546.
2. SOUMEUR, M.A., et al., *A Comparative Study of Two Energy Management Schemes for a Fuel-cell Hybrid Power System of Four-Wheel-Drive Electric Vehicle.* Journal of Power Technologies, 2021(1): p. 34-43%V 101.
3. Farkas, C., *Impact of uncoordinated electric vehicle charging on the distribution grid.* Journal of Power Technologies, 2020(1): p. 85-91%V 100.
4. Halder, S., et al. *Performance Analysis of WBG Inverter Fed Electric Traction Drive System for EV Application*. in *2023 IEEE IAS Global Conference on Renewable Energy and Hydrogen Technologies (GlobConHT)*. 2023. IEEE.
5. Popescu, M., et al., *Design of Induction Motors With Flat Wires and Copper Rotor for E-Vehicles Traction System.* IEEE Transactions on Industry Applications, 2023.
6. Shamsi-Nejad, M., M.R. Khalghani, and M.H. Khooban, *Determination of Optimum Hysteresis Bandwidth to Improve the Operation of Electric Machines.* Journal of Power Technologies, 2013(4): p. 207-215%V 93.
7. El Moucary, C., E. Mendes, and A. Razek, *Decoupled direct control for PWM inverter-fed induction motor drives.* IEEE transactions on industry applications, 2002. **38**(5): p. 1307-1315.
8. Nagarajan, R. and M. Saravanan. *Staircase multicarrier SPWM technique for nine level cascaded inverter*. in *2013 International Conference on Power, Energy and Control (ICPEC)*. 2013. IEEE.
9. Nashee, A.F., et al. *V/F control of AC motor using intelligent techniques*. in *AIP Conference Proceedings*. 2023. AIP Publishing.
10. Awdaa, M., A. Obed, and S. Yaqoob. *A Comparative Study between V/F and IFOC Control for Three-Phase Induction Motor Drives*. in *IOP Conference Series: Materials Science and Engineering*. 2021. IOP Publishing.
11. Ali, S.M., V.V.K. Reddy, and M.S. Kalavathi, *Coupled random PWM technique for dual inverter fed induction motor drive.* International Journal of Power Electronics and Drive Systems, 2019. **10**(1): p. 58.
12. Alsofyani, I.M. and N.R.N. Idris, *Simple flux regulation for improving state estimation at very low and zero speed of a speed sensorless direct torque control of an induction motor.* IEEE Transactions on power electronics, 2015. **31**(4): p. 3027-3035.
13. Velkov, T. and V. Chingoski, *SPEED CONTROL OF AC MOTORS FOR ELECTRIC VEHICLES USING FIELD ORIENTED CONTROL.* Balkan Journal of Applied Mathematics and Informatics, 2023. **6**(1): p. 37-48.
14. Kumar, R.S., et al., *A combined HT and ANN based early broken bar fault diagnosis approach for IFOC fed induction motor drive.* Alexandria Engineering Journal, 2023. **66**: p. 15-30.
15. Wang, Y., et al., *A comparative overview of indirect field oriented control (IFOC) and deadbeat-direct torque and flux control (DB-DTFC) for AC Motor Drives.* Chinese Journal of Electrical Engineering, 2015. **1**(1): p. 9-20.
16. Aktas, M., et al., *Direct torque control versus indirect field-oriented control of induction motors for electric vehicle applications.* Engineering Science and Technology, an International Journal, 2020. **23**(5): p. 1134-1143.

17. Amezquita-Brooks, L., J. Liceaga-Castro, and E. Liceaga-Castro, *Speed and position controllers using indirect field-oriented control: A classical control approach.* IEEE transactions on Industrial Electronics, 2013. **61**(4): p. 1928-1943.
18. Majeed, A.M.A., et al. *Investigation of SPWM and SVPWM VSI for Induction Motor Drive*. in *IOP Conference Series: Materials Science and Engineering*. 2020. IOP Publishing.
19. Wang, K., et al., *Modeling of system-level conducted EMI of the high-voltage electric drive system in electric vehicles.* IEEE Transactions on Electromagnetic Compatibility, 2022. **64**(3): p. 741-749.
20. Bhattacharjee, T., M. Jamil, and A. Jana. *Design of SPWM based three phase inverter model*. in *2018 Technologies for Smart-City Energy Security and Power (ICSESP)*. 2018. IEEE.
21. Hafeez, A., et al., *Comparative Analysis of the PWM and SPWM on Three-Phase Inverter through Different Loads and Frequencies.* Journal of Computing & Biomedical Informatics, 2023. **4**(02): p. 204-220.
22. Liang, W., et al., *Analytical modeling of current harmonic components in PMSM drive with voltage-source inverter by SVPWM technique.* IEEE Transactions on Energy Conversion, 2014. **29**(3): p. 673-680.
23. Singh, J., et al. *Investigation of performance parameters of PMSM drives using DTC-SVPWM technique*. in *2012 Students Conference on Engineering and Systems*. 2012. IEEE.
24. Rajlaxmi, E., S. Behera, and S.K. Panda. *Comparison of Inverter Control by SPWM and SVPWM Method in Standalone PV System*. in *2020 IEEE International Symposium on Sustainable Energy, Signal Processing and Cyber Security (iSSSC)*. 2020. IEEE.
25. Mathew, A.R., R. Bindu, and S. Thale. *Design of a power electronic drive for a small utility electric vehicle*. in *2020 IEEE India council international subsections conference (INDISCON)*. 2020. IEEE.
26. Jacob, J., et al. *Space vector pulse width modulation for a seven level inverter applied to an induction motor drive*. in *2017 International Conference on Innovations in Electrical, Electronics, Instrumentation and Media Technology (ICEEIMT)*. 2017. IEEE.
27. Katyara, S., A.A. Hashmani, and B.S. Chowdhary, *Development and analysis of pulse width modulation techniques for induction motor control.* Mehran University Research Journal of Engineering & Technology, 2020. **39**(1): p. 81-96.
28. Sudaryanto, A., et al. *Design and Implementation of SVPWM Inverter to Reduce Total Harmonic Distortion (THD) on Three Phase Induction Motor Speed Regulation Using Constant V/F*. in *2020 3rd International Seminar on Research of Information Technology and Intelligent Systems (ISRITI)*. 2020. IEEE.
29. Yadav, S. and A.K. Mishra. *Performance Evaluation in IFOC Induction Motor Drive with various PWM Techniques*. in *2020 International Conference on Electrical and Electronics Engineering (ICE3)*. 2020. IEEE.
30. Das, U., P.K. Biswas, and S. Debnath, *A Comparative Study between Load and No-Load condition of Brushless DC Motor Drives by Using MATLAB.* Journal of Power Technologies, 2017(3): p. 281–286%V 98.
31. Rind, S.J., et al., *Sliding mode control rotor flux MRAS based speed sensorless induction motor traction drive control for electric vehicles.* AIMS Electronics and Electrical Engineering, 2023. **7**(4): p. 354-379.
32. Haddoun, A., et al. *Sliding mode control of EV electric differential system*. in *ICEM'06*. 2006.
33. Haddoun, A., et al., *A loss-minimization DTC scheme for EV induction motors.* IEEE Transactions on vehicular technology, 2007. **56**(1): p. 81-88.
34. Yalavarthy, U.R.S. and V.S.K.R. Gadi, *Modelling, Simulation and Analysis of Indirect Space Vector Control of Electric Vehicle Driven by Permanent Magnet Synchronous Motor with Fuzzy Controller.* Mathematical Modelling of Engineering Problems, 2022. **9**(2).
35. Shah, K. and R. Maurya, *A modified space vector modulation based rotor flux oriented control of six-phase asymmetrical induction motor drive.* Turkish Journal of Electrical Engineering and Computer Sciences, 2023. **31**(2): p. 481-497.
36. Sirikan, P. and C. Charumit, *Implementation of indirect rotor field oriented control for three phase induction motor drive based on TMS320F28335 DSP.* Przegląd Elektrotechniczny, 2020. **96**: p. 153-158.

37. Bose, B.K., *Modern power electronics & AC drives*. 2002: Prentice hall.
38. Krishnan, R., *Electric Motor Drives: Analysis, Modeling and Control*. 2001, Prentice Hall Inc., New Jersey.
39. Ba-Razzouk, A., et al., *Field-oriented control of induction motors using neural-network decouplers.* IEEE Transactions on Power Electronics, 1997. **12**(4): p. 752-763.
40. Hiware, R.S. and J.G. Chaudhari. *Indirect field oriented control for induction motor*. in *2011 Fourth International Conference on Emerging Trends in Engineering & Technology*. 2011. IEEE.
41. Hamid, N.F.A., M.A. Abd Jalil, and N.S.S. Mohamed. *Design and simulation of single phase inverter using SPWM unipolar technique*. in *Journal of Physics: Conference Series*. 2020. IOP Publishing.
42. Jarjes, M.K. and T.A. Hussein, *Comparative study of SPWM and SVPWM techniques for the control of three-phase grid connected inverter.* Przeglad Elektrotechniczny, 2023. **99**(5).
43. Liu, K., Z. Zhou, and W. Hua, *A novel region-refinement pulse width modulation method for torque ripple reduction of brushless DC motors.* IEEE Access, 2018. **7**: p. 5333-5342.
44. Zhang, Z., et al., *PSCAD/EMTDC based SVPWM inverter simulation.* 2012.
45. Zhang, W.-F. and Y.-H. Yu, *Comparison of three SVPWM strategies.* Journal of Electronic Science and Technology, 2007. **5**(3): p. 283-287.
46. Miao, Y., et al., *Current Li-ion battery technologies in electric vehicles and opportunities for advancements.* Energies, 2019. **12**(6): p. 1074.
47. Khan, M.A., et al., *Performance analysis of bidirectional DC–DC converters for electric vehicles.* IEEE transactions on industry applications, 2015. **51**(4): p. 3442-3452.
48. Puranik, V.V. and V.N. Gohokar, *Simulation of an indirect rotor flux oriented induction motor drive using MATLAB/Simulink.* International Journal of Power Electronics and Drive Systems, 2017. **8**(4): p. 1693.
49. Sevilmiş, F. and H. Karaca. *Simulation and analysis of SVPWM based VSI for wind energy systems*. in *Proceedings of the 2014 6th International Conference on Electronics, Computers and Artificial Intelligence (ECAI)*. 2014. IEEE.
50. Chang, G.-W., et al., *Tuning rules for the PI gains of field-oriented controllers of induction motors.* IEEE Transactions on industrial electronics, 2000. **47**(3): p. 592-602.
51. Shukla, N.K. and R. Srivastava, *Simulation and Comparative Analysis of SPWM & SVPWM Based Voltage Source Inverter with Inductive Load.* Simulation, 2017.